Journal of *Marine Science and Engineering*

MDPI

Article

Prediction of the Pitch and Heave Motions in Regular Waves of the DTMB 5415 Ship Using CFD and MMG

Han-Bing Sun *, Shu-Qi Yang, Yang-Fan Xu and Jia-Feng Xiao

College of Shipbuilding Engineering, Harbin Engineering University, Harbin 150001, China
* Correspondence: sunhanbing@hrbeu.edu.cn

Abstract: According to the requirement of high-performance development of modern ships, it is necessary to quickly and accurately predict the maneuverability of ships under wave conditions. In this paper, based on the CFD (Computational Fluid Dynamics) method in the commercial software STAR-CCM+, the numerical simulation of roll decay motion, pure heel motion, pure heave motion, and pure pitch motion of ship model 5415 is carried out. The relevant hydrodynamic derivatives are obtained, and the results are in good agreement with the experimental values. The equations of motion related to the heave and pitch motions are established according to the MMG (Maneuvering Motion Equation Research Group) model. Then, based on the above dynamic equations, the wave force module is added to successfully simulate and predict the pitch and heave responses of the ship under regular wave conditions, and it is concluded that the simulation model for rapid prediction is also applicable under waves.

Keywords: vertical motions; hydrodynamic derivative; mathematical model group; regular waves; computational fluid dynamics

Citation: Sun, H.-B.; Yang, S.-Q.; Xu, Y.-F.; Xiao, J.-F. Prediction of the Pitch and Heave Motions in Regular Waves of the DTMB 5415 Ship Using CFD and MMG. *J. Mar. Sci. Eng.* **2022**, *10*, 1358. https://doi.org/10.3390/jmse10101358

Academic Editors: Dracos Vassalos and Kostas Belibassakis

Received: 31 August 2022
Accepted: 18 September 2022
Published: 22 September 2022

1. Introduction

With the increase of the speed of modern ships and the improvement of the accuracy of the ship's maneuverability prediction in complex sea conditions, the influence of the heave and pitch motion related to the vertical plane of the ship cannot be ignored. On this basis, the heave and pitch motion responses should be further considered, and the purpose of rapid prediction should be achieved.

Many scientists at home and abroad have carried out extensive research on the heave and pitch motion of ships, and have carried out numerical simulations of restraint ship model experiments (roll motion, pure heave motion, pure pitch motion, etc.) on the vertical plane of the ship. The MMG(Maneuvering Motion Equation Research Group) model in the mathematical model is widely used in the study of ship maneuverability and was proposed by the Japanese Ship Maneuvering Motion Equation Research Group(MMG), Inoue, Kijima and others [1,2] have done a lot of work in the study of disjunctive models. Bangun et al. [3] used the RANS(reynolds averaged navier-stokes equations) method to numerically simulate the forced rolling motion of the two-dimensional hull. Metin et al. [4] used the commercial software STAR CCM+ to numerically simulate the roll attenuation motion of the ship model 5415 with a bilge keel based on the dynamic deformation mesh technology, and the obtained roll damping coefficient was in good agreement with the experimental comparison. However, most of the current research on the motion of the ship in the vertical plane at home and abroad is to discuss the influence of different physical quantities on the motion itself. It is very expensive to solve the hydrodynamic derivatives related to pitch and heave through the experimental method. Few studies have been done on the effects of pitch and heave motions. Mei, T. et al. [5–14] Combined potential flow theory and computational fluid dynamics (CFD) technology to predict the maneuverability of ships in conventional waves, and the hull-related hydrodynamic derivatives were determined by using a two-body flow model using a RANS(reynolds averaged navier-stokes equations) solver. For maneuverability under waves, Chillcce et al. [15–20] took the DTC of a large container ship as the research object, used the three-dimensional Rankine source panel method to calculate the second-order wave force, and simulated the rotary motion of the ship in waves. The calculation results are in good agreement with the test. However, there are still few studies and comparisons on the manoeuvrability of the vertical plane of the ship under waves.

In this paper, the pitch motion of the vertical plane of the surface ship is studied. Based on the software STAR-CCM+, the vertical plane constrained motion of pure heave and pure pitch is numerically calculated, and the corresponding hydrodynamic derivatives are obtained and substituted according to the MMG (Maneuvering Motion Equation Research Group) model. In the established maneuvering motion equation, a simulation model of maneuverability prediction is established, and the fourth-order Runge–Kutta method is used to solve the maneuvering equation of motion to quickly predict the maneuverability of the ship, and the calculation results in still water are compared with the experimental values to verify the model effectiveness, so as to achieve the purpose of saving computing resources to a certain extent. The wave force module is added to the simulation model to explore the influence of waves on the maneuvering motion, so as to predict the ship maneuverability more comprehensively, accurately and quickly.

2. The Mathematical Model

The calculation object of this paper is the fully attached DTMB 5415 ship model, and the main parameters of its ship type, propeller, and rudder are shown in Table 1.

Table 1. Main parameters of the fully attached 5415 ship model.

Main Scale	Symbols and Units	Full Scale Model	Dimensions of the Boat Model
Scale ratio	λ	1	35.48
Length between vertical lines	L_{pp} (m)	142	4.002
type width	B (m)	19.06	0.538
draft	d (m)	6.15	0.173
drainage volume	∇ (m^3)	8424.4	0.189
Wetted surface area without rudder	S (m^2)	2972.6	2.361
Square coefficient	C_B	0.507	0.507
Middle cross-section coefficient	C_M	0.821	0.821
Longitudinal position of center of gravity (forward amidships is positive)	LCG	−0.652	−0.018
Vertical position of center of gravity (from baseline)	VCG (m)	7.54	0.213
Roll inertia radius	k_x/B	0.39	0.39
Pitch inertia radius	k_y/L_{pp}	0.255	0.255
moment of inertia around the z-axis	I_{ZZ} (kg·m^2)	1.27×10	225.3
High initial stability	GM (m)	1.95	0.055
rudder			
type		Spade	Spade
The total area	(m^2)	30.8	0.0245
side area	(m^2)	15.4	0.0122

To study the maneuverability of surface ships, a mathematical model of its motion should be first established. This article needs to use the separation model (MMG). The separation model (MMG) first separates the external forces of the ship into the hull hydrodynamic force, propeller force, and rudder force, and then considers the interference effect between each part. Assuming that the ship is a rigid body, according to the rigid body center-of-mass motion theory and the separation modeling idea, when only the pitch-heave motion is considered, the three-degree-of-freedom maneuvering motion equation of the vertical plane can be established:

$$\begin{cases} m(\dot{v}+ur-\omega p)=Y_H+Y_P+Y_R+Y_W \\ m(\dot{\omega}-uq+vp)=Z_H+Z_P+Z_R+Z_W \\ I_{XX}\dot{p}+(I_{ZZ}-I_{YY})qr=K_H+K_P+K_R+K_W \\ I_{YY}\dot{q}+(I_{XX}-I_{ZZ})pr=M_H+M_P+M_R+M_W \\ I_{ZZ}\dot{r}+(I_{YY}-I_{XX})pq=N_H+N_P+N_R+N_W \end{cases} \tag{1}$$

where m is the mass of the hull; $I_{XX},\ I_{YY},\ I_{ZZ}$ are the moments of inertia of the hull mass around the x, y, and z axes, respectively; $\dot{u},\ \dot{v},\ \dot{\omega}$ are the longitudinal, lateral, and vertical accelerations of the hull, respectively; $\dot{p},\ \dot{q},\ \dot{r}$ are the roll, pitch, and yaw accelerations of the hull, respectively. Among them, the subscripts $H,\ P,\ R,\ W$ are the hydrodynamic force of the hull, the force of the propeller, the force of the rudder, and the force (moment) of the wave acting on the hull. The hydrodynamic force on the hull itself can be divided into an inertial hydrodynamic force and a viscous hydrodynamic force according to its properties. The hull hydrodynamic force can be expressed as:

$$\begin{cases} Y_H=Y_{HI}+Y_{HV} \\ Z_H=Z_{HI}+Z_{HV} \\ K_H=K_{HI}+K_{HV} \\ M_H=M_{HI}+M_{HV} \\ N_H=N_{HI}+N_{HV} \end{cases} \tag{2}$$

where the subscripts HI and HV represent the inertial hydrodynamic and viscous hydrodynamics of the hull, respectively.

The additional hydrodynamic force that the ship will experience when it performs unsteady motion in the fluid is the inertial hydrodynamic force of the hull. Its direction is opposite to the direction of the motion acceleration, and its magnitude is proportional to the acceleration. This proportionality factor is the additional mass (additional moment of inertia). Considering the symmetry of the ship and the neglect of the smaller order terms, the inertial hydrodynamic equation after a certain simplification is as follows:

$$\begin{cases} -Y_{HI}=m_y\dot{v}+m_xur-m_z\omega p \\ -Z_{HI}=m_z\dot{\omega}-m_xuq+m_yvp \\ -K_{HI}=J_{XX}\dot{p}+(J_{ZZ}-J_{YY})qr+(m_z-m_y)v\omega \\ -M_{HI}=J_{YY}\dot{q}+(J_{XX}-J_{ZZ})pr+(m_x-m_z)u\omega \\ -N_{HI}=J_{ZZ}\dot{r}+(J_{YY}-J_{XX})pq \end{cases} \tag{3}$$

where $m_x,\ m_y,\ m_z$ are the additional mass of the hull in the axial direction, respectively; $J_{XX},\ J_{YY},\ J_{ZZ}$ are the additional moment of inertia of the hull rotating around the axis $x,\ y,\ z$.

Combined with the improved MMG (Maneuvering Motion Equation Research Group) model of Umeda et al. [21], the viscous hydrodynamic force is expressed as:

$$\begin{cases} Y_{HV}=Y_v v+Y_{vvv}v^3+Y_r r+Y_{rrr}r^3+Y_{vrr}vr^2+Y_{vvr}v^2r+Y_\phi\phi \\ Z_{HV}=Z(u)+Z_\omega\omega+Z_q q+Z_z z+Z_\theta\theta \\ K_{HV}=K_p p-mg\overline{GZ}+K_\phi\phi-Y_{HV1}z_H \\ M_{HV}=M(u)+M_\omega\omega+M_q q+M_z z+M_\theta\theta \\ N_{HV}=N_v v+N_{vvv}v^3+N_r r+N_{rrr}r^3+N_{vrr}vr^2+N_{vvr}v^2r+N_\phi\phi \end{cases} \tag{4}$$

where z_H is the vertical coordinate of the point of action of the lateral force; $\overline{GZ}=GM\sin\phi$ is the stability arm, GM is the initial high stability; g is the gravitational acceleration. From the above formulas, it can be seen that the calculation of the hull hydrodynamics is actually the solution of the hydrodynamic derivatives. In this paper, the CFD technology is used to simulate the constrained ship model test to solve the above-mentioned hydrodynamic derivatives. Table 2 shows the hydrodynamic derivatives that can be calculated for the rocking motion.

Table 2. The source of the hydrodynamic derivative.

Hydrodynamic Derivative	Source
K_p, J_{XX}	roll decay motion
Y_ϕ, K_ϕ, N_ϕ	pure heel motion
Z_ω, Z_z, M_ω, M_z, m_z	pure heave motion
Z_q, Z_θ, M_q, M_θ, J_{YY}	pure pitch motion

3. Numerical Computation Method

3.1. Governing Equations

In this paper, the CFD method is used to simulate the hydrodynamics of the ship, and the Navier–Stokes equations in the viscous flow field are numerically solved, and the Reynolds-averaged Navier–Stokes equations (RANS) equations are used to approximate the viscous flow field. By averaging the random pulsation terms in the viscous flow field, the unsteady problem is transformed into a steady problem. The continuity equation for viscous flow is as follows:

$$\frac{\partial \rho}{\partial t} + \frac{\partial(\rho u_i)}{x_i} = 0 \tag{5}$$

The Reynolds-averaged Navier–Stokes (RANS) equations are:

$$\frac{\partial(\rho u_i)}{\partial t} + \frac{\partial(\rho u_i u_j)}{x_i} = -\frac{\partial p}{\partial x_i} + \frac{\partial}{x_i}(\mu \frac{\partial u_i}{\partial x_j} - \rho\overline{u_i' u_j'}) + s_i \tag{6}$$

where $\rho u_i u_j$ is the Reynolds stress term, ρ is the density; μ is the dynamic viscosity coefficient; p is the time-averaged pressure; u_i, u_j is the time-averaged velocity component (i, j = 1, 2, 3).

The equation for the turbulent kinetic energy k is:

$$\frac{\partial}{\partial t}(\rho k) + \frac{\partial}{\partial x_i}(\rho k u_i) = \frac{\partial}{\partial x}\left(\Gamma_k \frac{\partial k}{\partial x_j}\right) + G_k - Y_k + S_k \tag{7}$$

The equation for the turbulent dissipation rate ω is:

$$\frac{\partial}{\partial t}(\rho \omega) + \frac{\partial}{\partial x_j}(\rho \omega u_i) = \frac{\partial}{\partial x}\left(\Gamma_\omega \frac{\partial \omega}{\partial x_j}\right) + G_\omega - Y_\omega + D_k + S_\omega \tag{8}$$

where the G_ω is the turbulent dissipation rate; Y_k, Y_ω are the turbulent diffusion terms; S_k, S_ω are the self-defined source terms; Γ_k, Γ_ω are the diffusivity of k and ω; G_k is the turbulent kinetic energy formed by the average velocity gradient.

In this paper, the above method is used to carry out the numerical simulation of the pitch-heave motion of the surface ship, and the relevant hydrodynamic derivatives are obtained by regression, and the maneuvering motion is predicted. The pitch-heave motion numerical simulation includes the following motion forms: roll decay motion, pure heel motion, pure heave motion, and pure pitch motion.

3.2. Computational Domain and Boundary Condition Settings

The division of the computational domain and the setting of boundary conditions are shown in Figures 1 and 2. The entire computational domain is divided into an overlapping area and a background area. The settings of the overlapping domain are: the front end is 0.25 times the length of the ship from the bow, the rear part is 0.25 times the length of the ship from the stern, the side boundary is 0.2 times the length of the ship from the mid-ship longitudinal section, and the upper and lower boundaries are 0.225 times the length of the ship and 0.15 times the length of the ship from the keel. The boundary entrance is 1.5 times the length of the length from the bow, the boundary exit is 3.5 times the length of the ship from the stern, the side of the boundary is 1.5 times the length of the ship from the mid-ship longitudinal section, and the upper and lower boundaries are 2/3 times the length and 4/3 times the length of the ship from the keel, respectively.

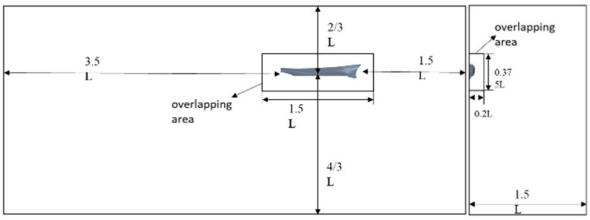

Figure 1. The division of computing area.

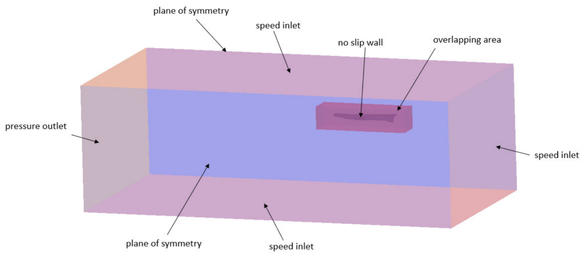

Figure 2. Setting of boundary conditions.

3.3. Meshing and Convergence Analysis

The entire watershed is divided by the cutting body mesh, and the mesh is refined for the part of the hull with large curvature changes, such as the overlapping area, the free surface, the bow and stern, and the bilge keel. The size of the overlapping grid area should be consistent with the grid size of the surrounding refinement area to ensure the calculation accuracy. In order to determine the influence of grid size on the calculation results and verify the effectiveness of the grid scheme, the straight-line motion when Fr = 0.28 was taken as the research object, and the grid convergence analysis was carried out.

In the grid convergence analysis, the stability of the calculation result is judged by the convergence parameter R_G, which is defined as follows:

$$R_G = \frac{S_2 - S_1}{S_3 - S_2} \tag{9}$$

In the formula: S_1, S_2, S_3 are the calculation results of fine grid, medium grid and coarse grid, respectively; R_G is the convergence parameter, when $0 < R_G < 1$, the results are uniformly convergent.

It can be seen from Table 3 that the calculation results are consistent and convergent, and gradually stabilize with the increase of the number of grids. The agreement is good, and the calculation accuracy is high. In order to improve the computational efficiency while taking into account the computational accuracy, a medium grid simulation is adopted. Therefore, the grid division is shown in the Figure 3 below, the number of grid cells in the overlapping area is 1.83 million, and the number of grid cells in the background area is 1.29 million.

Table 3. Convergence analysis with different mesh sizes.

Grid Sizes	Grid Amount (Million)	CFD (N)	EFD (N)	E (%)
fine	2.46	18.416	18.41	0.03
medium	1.1	18.534	18.41	0.67
coarse	0.56	18.821	18.41	2.23
R_G		0.41		

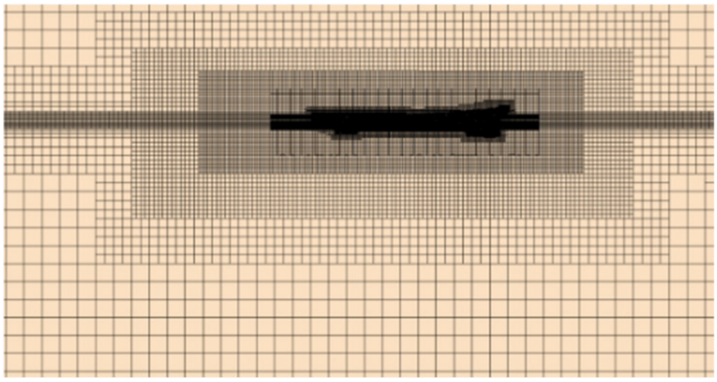

Figure 3. The grid division.

4. Results of Hydrodynamic Derivative

4.1. Numerical Simulation of Roll Decay Motion

The roll decay motion refers to the motion that the ship freely rolls with an initial heel angle in still water until the roll amplitude decays to 0. The roll extinction curve is obtained by numerically simulating the roll decay motion, and the corresponding hydrodynamic derivative and additional inertia moment are finally regressed. According to the linear assumption, the roll extinction curve can be fitted to the following equation:

$$\Delta\phi = a\phi_m \tag{10}$$

In the formula: a is the extinction coefficient; $\Delta\phi$ and ϕ_m are the difference and the average value of the adjacent two roll amplitudes, respectively. It should be pointed out that the unit here is degree.

According to the energy conservation relationship, the relationship between the hydrodynamic derivative of the roll angular velocity (that is, the roll damping coefficient) K_p and the extinction coefficient a can be obtained as follows:

$$a = -\frac{\pi}{2}\frac{\omega_\phi}{DGM}K_p \tag{11}$$

where D is the weight of the ship; GM is the high initial stability of the ship; ω_ϕ is the natural frequency of rolling, which can be obtained from the measured rolling period T.

The total moment of inertia of the ship around the x-axis can be obtained from the natural frequency of rolling:

$$\omega_\phi = \sqrt{\frac{DGM}{I_{xx} + J_{xx}}} \tag{12}$$

where $I_{xx} + J_{xx}$ is the sum of the moment of inertia of the ship around the x-axis and the additional moment of inertia, that is, the total moment of inertia. The calculation conditions are shown in the Table 4 below.

Table 4. Calculation cases of roll decay motion.

F_r	U (m/s)	Initial Heel Angle (°)
0.28	1.751	2.5, 5, 7.5, 10

The roll attenuation curves and roll extinction curves of different heel angles are shown in Figures 4 and 5. The roll angle gradually decreases with the increase of time. The larger the initial heel angle, the faster the attenuation. The roll decay period is also different, which may be related to the influence of the initial heel angle on the roll damping coefficient K_p, and the extinction coefficient a decreases with the gradual decrease of the initial heel angle.

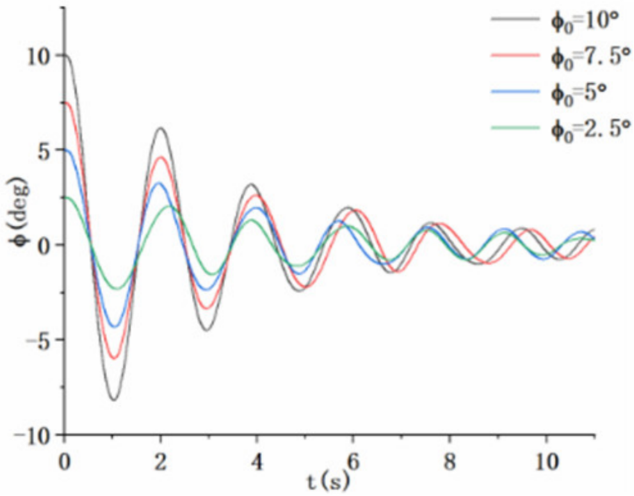

Figure 4. The roll attenuation curves.

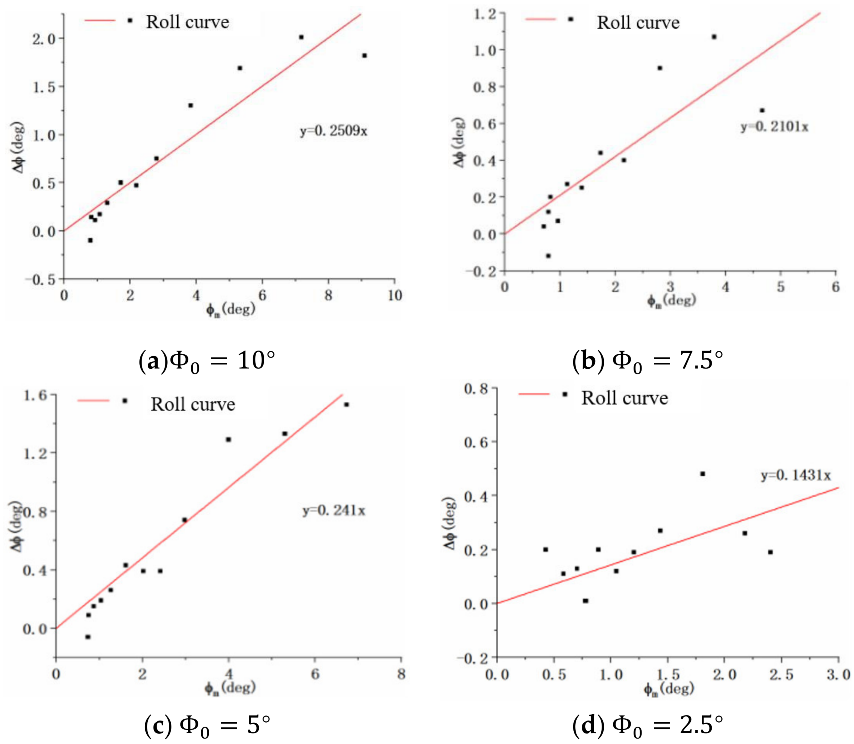

Figure 5. The roll extinction curves.

As shown in Figure 6, the hydrodynamic derivative of the roll angular velocity K_p at different initial heel angles increases with the increase of the initial heel angle, which is also the main reason why the increase in initial heel angle leads to faster roll decay. In addition, the least squares method is used to perform quadratic fitting on the calculation results to obtain the hydrodynamic parameters related to the roll decay motion, as shown in Table 5.

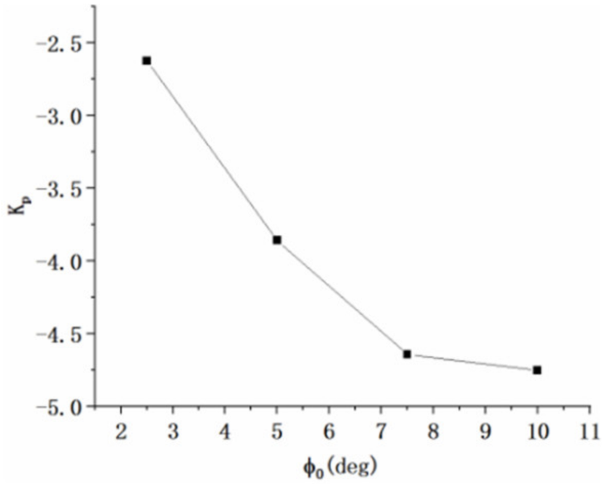

Figure 6. The hydrodynamic derivative of the roll angular velocity K_p at different initial heel angles.

Table 5. Hydrodynamic parameters related to the roll decay motion.

Parameter	CFD	EFD	E (%)
K_p	−3.94	−3.81	3.41
T	1.83	1.75	4.57

4.2. Numerical Simulation of Pure Heel Motion

The pure heel motion is the uniform straight-line dragging motion of the ship in the pool at a certain heel angle. The corresponding hydrodynamic derivatives in the maneuverability equation of motion are obtained by measuring different heeling force, rolling moment, and yaw moment and then regressing. The dynamic model is as follows:

$$\begin{cases} Y = Y_\phi \phi \\ K = K_\phi \phi \\ N = N_\phi \phi \end{cases} \tag{13}$$

where ϕ is the heel angle, and the calculation conditions of pure heel motion in this section are shown in the Table 6 below.

Table 6. Calculation cases of pure heel motion.

Fr	***U* (m/s)**	**ϕ (°)**
0.28	1.751	0, 5, 10, 15, 20

The following Figure 7 shows the calculation results under different working conditions. The roll moment is greatly affected by the heel angle, while the roll force and the bow moment are less affected. Using the least squares method, the hydrodynamic derivative can be obtained by regression as shown in the following table. It can be seen that the hydrodynamic derivative (Table 7) of the lateral force with respect to the heeling motion is very small and can be ignored.

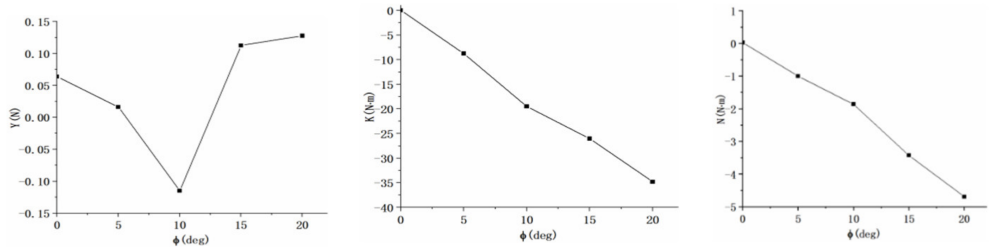

(**a**) Lateral force (**b**) Roll moment (**c**) Yaw moment

Figure 7. Calculation results of pure heel motion.

Table 7. Hydrodynamic parameters related to pure heel motion.

Hydrodynamic Derivatives	Value
Y_ϕ	0.004234
K_ϕ	−1.767
N_ϕ	−0.2252

4.3. Numerical Simulation of Pure Heave Motion

Pure heave motion refers to the motion in which the ship model moves in a straight line at a uniform speed in the longitudinal direction and superimposes a sinusoidal vertical displacement in the vertical direction, and the trim angle is always zero.

The equation of motion for pure heave motion is as follows:

$$\begin{cases} \theta = 0 \\ z = z_{\max} \sin wt = a \sin wt \\ \omega = \omega_{\max} \cos wt = aw \cos wt \\ \dot{\omega} = -\dot{\omega}_{\max} \sin wt = -aw^2 \sin wt \end{cases} \tag{14}$$

where θ is the pitch angle; a is the amplitude of a vertical harmonic oscillation; w is the circular frequency of a simple harmonic motion ($w = 2\pi f$); f is the frequency of a simple harmonic motion; z is the vertical displacement: ω is the vertical velocity; $\dot{\omega}$ is the vertical acceleration, where the subscript max represents the magnitude. The hydrodynamic equations of the corresponding surface ships are as follows:

$$\begin{cases} Z = Z(u) + Z_\omega \omega + Z_{\dot{\omega}} \omega + Z_z z \\ M = M(u) + M_\omega \omega + M_{\dot{\omega}} \omega + M_z z \end{cases} \tag{15}$$

In the formula (15): $Z_{\dot{\omega}}$, $M_{\dot{\omega}}$ are the hydrodynamic derivatives of the vertical acceleration, among them, $Z_{\dot{\omega}} = -m_z$; the magnitude of $M_{\dot{\omega}}$ is small and generally ignored in the mathematical model of the MMG maneuvering motion; $Z(u)$, $M(u)$ are the functions of the vertical force and pitch moment on the speed, respectively, and at a fixed speed, they are constant; Z_z, M_z are the hydrodynamic derivatives of vertical displacement, namely the derivatives of restoring force and moment.

Substituting the motion parameters of Equation (14) into Equation (15), the expansion can be obtained as:

$$\begin{cases} Z = Z(u) + Z_\omega aw \cos wt + \left(aZ_z - aw^2 Z_{\dot{\omega}}\right) \sin wt \\ M = M(u) + M_\omega aw \cos wt + \left(aM_z - aw^2 M_{\dot{\omega}}\right) \sin wt \end{cases} \tag{16}$$

According to formula (16), the corresponding coefficients obtained by Fourier function fitting are as follows:

$$\begin{cases} Z_{C1} = Z_\omega aw \\ Z_{S1} = aZ_z - aw^2 Z_{\dot{\omega}} \\ M_{C1} = M_\omega aw \\ M_{S1} = aM_z - aw^2 M_{\dot{\omega}} \end{cases} \tag{17}$$

According to the Fourier coefficient in Equation (17), the hydrodynamic derivative is obtained by further fitting with the least squares method.

The calculation conditions of pure heave motion are shown in the Table 8 below, and the motion conditions at different speeds and different frequencies are calculated.

Table 8. Calculation cases of pure heave motion.

F_r	a (m)	f (HZ)
0.138, 0.28, 0.41	0.01	0.1, 0.15, 0.2, 0.25, 0.4, 0.6

Figure 8 shows the time-history curves of the vertical force and pitch moment in a period of pure heave motion with different oscillation frequencies at different speeds. It can be seen that regardless of the speed, the vertical force of the pure heave motion of the ship model at different frequencies generally decreases with the increase of the frequency. The vertical force will be affected by the speed of the ship. Under the same frequency, the vertical force fluctuates more obviously with the increase of the speed. It can also be seen that the curve of pitch moment has obvious changes in amplitude or phase difference with the increase of speed and frequency.

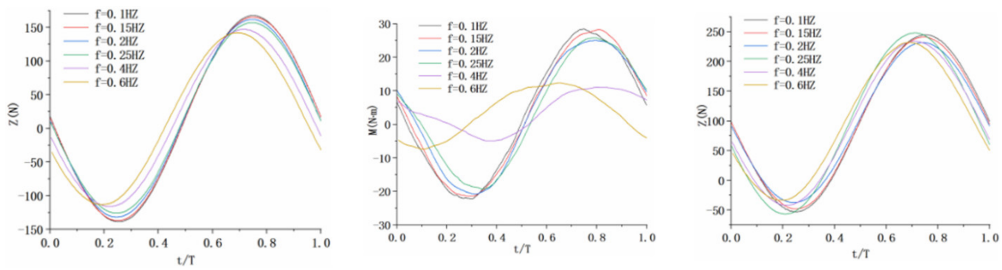

(**a**) Fr = 0.138 (**b**) Fr = 0.138 (**c**) Fr = 0.28

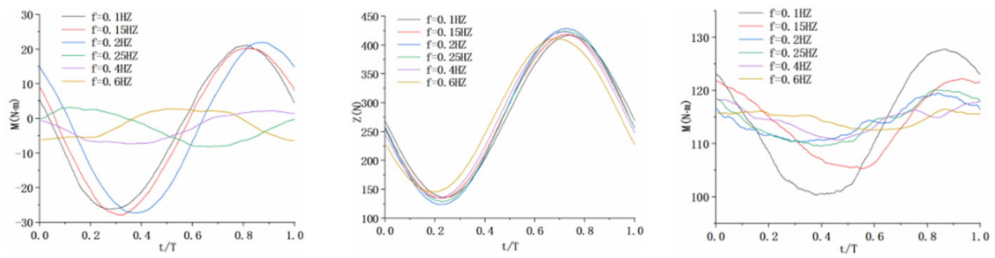

(**d**) Fr = 0.28 (**e**) Fr = 0.41 (**f**) Fr = 0.41

Figure 8. The time-history curves of the vertical force and pitch moment.

Table 9 shows the calculation results of the hydrodynamic derivatives of pure heave motion at different speeds. Due to the large difference between the calculation results at different speeds, the hydrodynamic derivatives at different speeds are divided into three hydrodynamic derivatives to represent the hydrodynamic derivatives of the low, medium and high-speed sections, respectively. So, it is used in the manipulative motion equation.

Table 9. Hydrodynamic parameters related to pure heave motion.

Hydrodynamic Derivatives	*Fr* = 0.138	*Fr* = 0.28	*Fr* = 0.41
Z_ω	−1590	−1517	−1108
Z'_ω	−5.316	−2.503	−1.246
$Z_{\dot{\omega}}$	−239.8	−160	−134.2
$Z'_{\dot{\omega}}$	−0.173	−0.115	−0.097
	−15,050	−14,560	−14,590
Z'_z	−233.074	−54.900	−25.557
M_ω	−351.4	−485.6	−231.7
M'_ω	−0.294	−0.200	−0.065
$M_{\dot{\omega}}$	−145.3	−121.5	−45.2
$M'_{\dot{\omega}}$	−0.026	−0.022	−0.008
M_z	−2373	−1570	−491.1
M'	−9.183	−1.479	−0.215

4.4. Numerical Simulation of Pure Pitch Motion

When the ship is in pure pitch motion, the ship model moves at a uniform longitudinal speed while superimposing a cosine-varying trim angle, and the ship's motion trajectory is tangent to the longitudinal axis of the ship.

The equation of motion for pure pitch motion is as follows:

$$\begin{cases} \theta_{\max} = \frac{aw}{U} \\ \theta = -\theta_{\max}\cos wt \\ q = q_{\max}\sin wt = \theta_{\max} w \sin wt \\ \dot{q} = \dot{q}_{\max}\cos wt = \theta_{\max} w^2 \cos wt \end{cases} \tag{18}$$

where q is the pitch angular velocity; $\dot{q}$ is the pitch angular acceleration, where the subscript *max* represents the amplitude.

Similarly, for the pure heave motion of surface ships, the hydrodynamic equation of pure pitch motion also needs to add restoring force and moment terms. The simplified hydrodynamic equation is as follows:

$$\begin{cases} Z = Z(u) + Z_q q + Z_{\dot{q}}\dot{q} + Z_\theta \theta \\ M = M(u) + M_q q + M_{\dot{q}}\dot{q} + M_\theta \theta \end{cases} \tag{19}$$

In the formula (19): $Z_{\dot{q}}$, $M_{\dot{q}}$ are the hydrodynamic derivatives of the pitch angular acceleration, among which, $M_{\dot{q}} = -J_{YY}$; the magnitude of $Z_{\dot{q}}$ is small and generally ignored in the mathematical model of the MMG maneuvering motion; Z_θ, M_θ are the hydrodynamic derivatives related to the pitch angle, that is, the restoring force and moment derivatives.

Substituting the motion parameters of Equation (18) into Equation (19), it can be further expanded and expressed as:

$$\begin{cases} Z = Z(u) + Z_q \theta_{\max} w \sin wt + \left(Z_{\dot{q}} \theta_{\max} w^2 - \theta_{\max} Z_\theta \right) \cos wt \\ M = M(u) + M_q \theta_{\max} w \sin wt + \left(M_{\dot{q}} \theta_{\max} w^2 - \theta_{\max} M_\theta \right) \cos wt \end{cases} \tag{20}$$

According to formula (20), the corresponding Fourier coefficients are obtained by fitting the Fourier function as follows:

$$\begin{cases} Z_{C1} = Z_{\dot{q}} \theta_{\max} w^2 - \theta_{\max} Z_\theta \\ Z_{S1} = Z_q \theta_{\max} w \\ M_{C1} = M_{\dot{q}} \theta_{\max} w^2 - \theta_{\max} M_\theta \\ M_{S1} = M_q \theta_{\max} w \end{cases} \tag{21}$$

According to the Fourier coefficient in the formula (21), the required hydrodynamic derivative can be obtained by further fitting with the least square method.

This section numerically simulates pure pitch motion at different speeds and frequencies. The calculation conditions are shown in the Table 10 below. The pure pitch motion is similar to the pure heave motion, and is still realized by the plane motion mechanism of the DFBI (*Dynamic Fluid Body Interaction*).

Table 10. Calculation cases of pure pitch motion.

Fr	*a* (m)	*f* (HZ)
0.138, 0.28, 0.41	0.01	0.1, 0.15, 0.2, 0.25, 0.4, 0.6

The time-history curves of the vertical force and pitch moment of pure pitch motion calculated under the above different working conditions are shown in the Figure 9, and the change is similar to that of pure heave motion. As the speed increases, the change curve of the vertical force moves upward as a whole. However, with the increase of frequency, the amplitude of vertical force is not as obvious as that of pure heave motion. The pitch moment also changes periodically. When the frequency is constant and the speed increases, the strength curve of the pitch moment first moves down and then up. In the case of the same speed at different frequencies, the pitch moment does not change significantly, and the amplitude increases as the frequency increases.

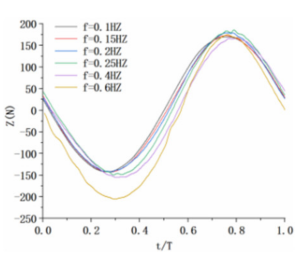

(**a**) Fr = 0.138

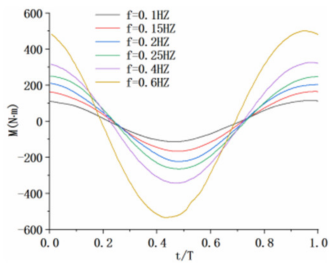

(**b**) Fr = 0.138

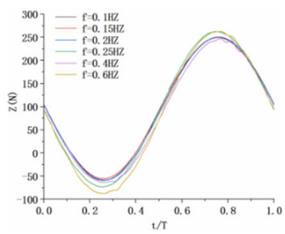

(**c**) Fr = 0.28

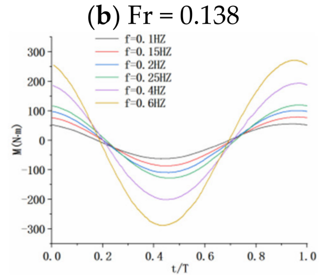

(**d**) Fr = 0.28

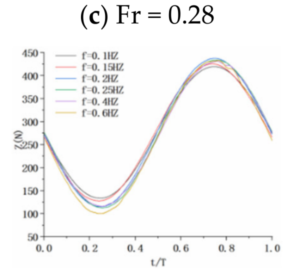

(**e**) Fr = 0.41

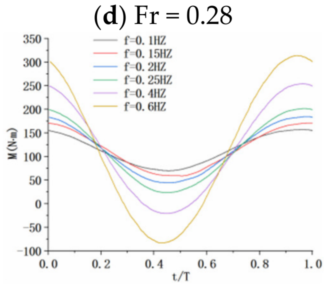

(**f**) Fr = 0.41

Figure 9. The time-history curves of the vertical force and pitch moment.

The calculation results of the hydrodynamic derivatives of pure pitch motion are shown in Table 11. As in the case of pure heave motion, a piecewise function needs to be used to describe the hydrodynamic derivatives of the three speeds.

Table 11. Hydrodynamic parameters related to pure pitch motion.

Hydrodynamic Derivatives	***Fr* = 0.138**	***Fr* = 0.28**	***Fr* = 0.41**
Z_q	–	−241.1	−268.7
Z'_q	−0.124	−0.099	−0.075
$Z_{\dot{q}}$	−82.35	−40.04	12.76
$Z'_{\dot{q}}$	−0.015	−0.007	0.002
Z_θ	−2152	−1133	240.2
Z'_θ	−8.328	−1.067	0.105
	−989.2	−982.8	−1153
M'_q	−0.207	−0.101	−0.081
$M_{\dot{q}}$	−198.4	−145.2	−146.6
$M'_{\dot{q}}$	−0.009	−0.007	−0.007
M_θ	−13,860	−14,220	−14,580
M'_θ	−13.402	−3.348	−1.595

The simulation of the vertical plane kinematic mechanism does not fit the functions of $Z(u)$, $M(u)$ because the calculated speed is less. In order to obtain a more accurate $Z(u)$, $M(u)$, and reference $X(u)$ fitting, the straight motion should be numerically simulated without releasing the heave and trim degrees of freedom at different speeds, and the vertical force and trim moment of the ship model are obtained, so that the combined function of $Z(u)$ and $M(u)$ is fitted. The result is shown in the Figure 10 below.

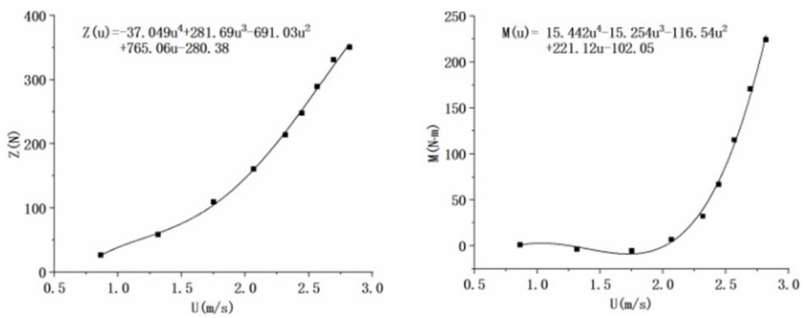

(a) $Z(u)$ **(b)** $M(u)$

Figure 10. Fitting results.

5. Results of Motion Simulation

The constrained ship model simulation method based on CFD (Computational Fluid Dynamics) is to use the CFD numerical simulation of ship model constrained motion regression to obtain the corresponding hull hydrodynamic derivative, combined with the ship's MMG mathematical model, and construct the ship's maneuverability motion simulation model to predict the ship's maneuverability. In this paper, the fourth-order Runge–Kutta method is used to obtain the mathematical model of the ship's maneuvering motion. After calculating the acceleration of the ship at each time, the acceleration is numerically integrated to obtain the speed and position of the ship at each time, so as to predict the ship's maneuvering motion. After the calculation model is established, the calculation results in the still water state are compared with the test results to verify the reliability of the model. The maneuverability prediction results with the addition of the wave force module are also calculated, indicating that the influence of waves on maneuverability of the ship cannot be ignored.

5.1. Validation in Calm Water

Figure 11 shows the comparison between the simulation model calculation results and the experimental values under straight sailing motion. It can be seen that as the speed increases, the heave displacement of the hull increases, and the trim angle decreases first and then increases. Table 12 shows the error between the simulation results and the experimental values of the hull trim angle and heave value. The simulation results are in good agreement with the experimental values. The error range varies from 0.68% to 40%. Only when Fr = 0.138, the error of the trim angle is slightly larger. The pitch angle change is very small at low speed, and even a small change will make the error appear larger when the value is too small. However, the numerical simulation and experimental values of the ship's trim angle and heave have the same overall trend, which verifies the effectiveness of the method based on CFD to calculate the constrained motion of the ship model to obtain the hydrodynamic derivative. Compared with the method of CFD, it takes only a few seconds to complete a working condition through numerical simulation, which greatly improves the calculation efficiency, and can provide a method reference for the subsequent ship maneuverability forecast.

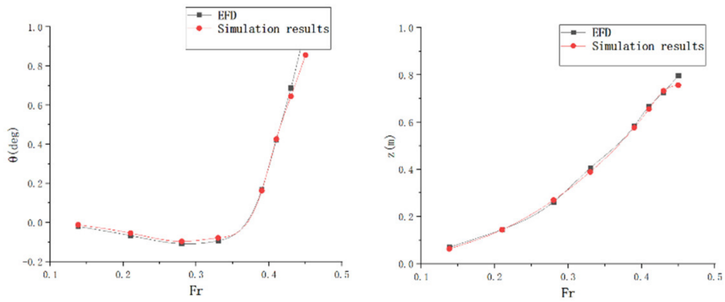

(**a**) pitch (**b**) heave

Figure 11. The comparison between the simulation model calculation results and the experimental values.

Table 12. The comparison between the simulation model calculation results and the experimental values.

Fr	The Error of Pitch Angle/%	The Error of Heave Value/%
0.138	40	9.86
0.21	19.4	0.68
0.28	11.1	2.66
0.33	16.1	3.94
0.39	2.98	1.20
0.41	0.95	1.65
0.43	6.25	0.83
0.45	14.4	5.14

5.2. Response in Waves

As shown in the Figure 12, the wave force module is added to the above simulation mathematical model. Under different sea conditions, the pitch angle and heave value change with the encounter frequency at different speeds. It can be seen that the pitch angle at the same speed changes as a trigonometric function with the change in the encounter frequency. It can also be seen that under the same encounter frequency, with the increase of the speed, the changes in the low-speed section are relatively similar, and the change range is much larger at high speed. The heave value of the ship at the same speed generally decreases with the increase of the encounter frequency, and it is also a fluctuation change of an approximate trigonometric function. Under the same encounter frequency, it can be seen that the heave value of the ship increases with the increase of the speed, and the heave value changes more sharply at high speed. It can be seen that the simulation model under the action of waves can still predict the maneuverability of the ship, and it shows that the influence of the vertical motion of the ship cannot be ignored.

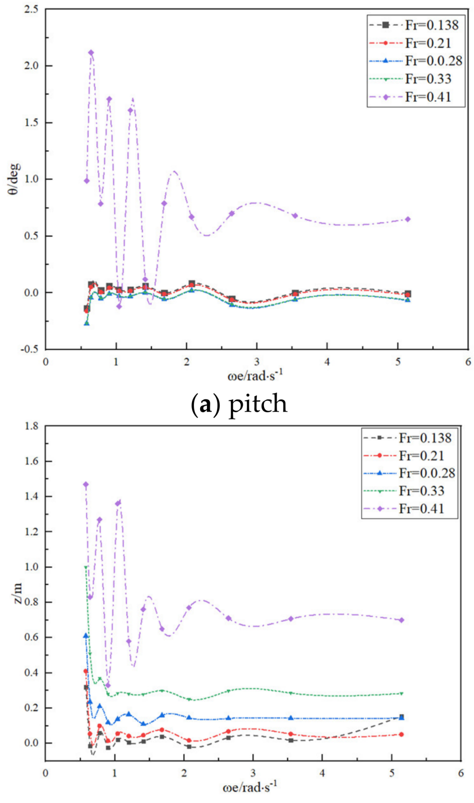

(**a**) pitch

(**b**) heave

Figure 12. Calculation results under waves.

6. Conclusions

This paper firstly divided the computational watershed grid based on the overlapping grid method of CFD (Computational Fluid Dynamics), and established a numerical calculation model. Then, based on the established model, the roll attenuation motion of the ship model 5415 under different initial heel angles was simulated, and the roll attenuation curves under different initial heel angles were calculated, and the roll extinction curves under different initial heel angles were drawn. The hydrodynamic derivatives at different initial heel angles were further regressed using the least squares method to obtain more accurate hydrodynamic derivatives, and the results were in good agreement with the experiments. Afterwards, the pure heel motion, pure heave and pure pitch motion of the ship model 5415 were simulated using the dynamic grid numerical scheme, the straight sailing motion under different fixed heel angles was calculated, and its hydrodynamic performance was analyzed, including the effect of the heel angle on the lateral force, rolling moment, and yaw moment, and regressed to obtain the hydrodynamic derivative related to pure heel motion. Then, the influence of the changes of the speed and frequency on the vertical force and pitch moment of the pure heave and pure pitch motion of the ship model 5415 at different speeds and different frequencies was calculated, and at the same time, regressed to obtain the corresponding hydrodynamic derivatives and analyze the effect of the speed on the water. The effect of the dynamic derivative was used to obtain the vertical force and pitch moment as a function of the speed of the ship. In addition, the flow field information around the hull under different working conditions was also analyzed, and the action mechanism of the hull hydrodynamics in the vertical plane restraint motion was discussed. Finally, the fourth-order Runge–Kutta solution of the motion equation formed by solving the hydrodynamic derivative of the ship model constrained motion was carried out, and the comparison with the experimental value verified the effectiveness of the numerical simulation for maneuverability prediction. The wave force was added to the simulation module, and the pitch and heave values were compared with the change of the encounter frequency and the speed of the ship under the wave. It was found that the simulation model can also predict the maneuverability under the wave. In addition, it was found that the vertical motion of the ship is relatively large when the ship moves under the waves, so the influence of the vertical motion of the ship when sailing in the waves cannot be ignored.

This article provides a research basis for the fitting of empirical formulas about hydrodynamic derivatives in the future, and also provides a reference for rapid forecasting of more types of ships under waves.

Author Contributions: Conceptualization and methodology, H.-B.S.; software, S.-Q.Y.; validation, J.-F.X.; formal analysis, S.-Q.Y.; investigation, Y.-F.X.; resources, Y.-F.X.; data curation, Y.-F.X.; writing—original draft preparation, writing—review and editing, S.-Q.Y.; visualization, S.-Q.Y.; supervision, H.-B.S.; project administration, H.-B.S.; funding acquisition, H.-B.S. All authors have read and agreed to the published version of the manuscript.

Funding: The authors gratefully acknowledge the support of the National Natural Science Foundation of China (Grant No. 52071100 and No. 51739001).

Conflicts of Interest: The authors declare no conflict of interest.

References

1. Inoue, S.; Hirano, M.; Kijima, K. Hydrodynamic derivatives on ship manoeuvring. *Int. Shipbuild. Progress* **1981**, *28*, 112–125. [CrossRef]
2. Kijima, K. Some studies on the prediction for ship manoeuvrability. In Proceedings of the International Conference on Marine Simulation and Ship Manoeuvrability, Kanazawa, Japan, 25–28 August 2003.
3. Bangun, E.P.; Wang, C.M.; Utsunomiya, T. Hydrodynamic forces on a rolling barge with bilge keels. *Appl. Ocean Res.* **2010**, *32*, 219–232. [CrossRef]
4. Gokce, M.K.; Kinaci, O.K. Numerical simulations of free roll decay of DTMB 5415. *Ocean Eng.* **2018**, *159*, 539–551. [CrossRef]
5. Mei, T.; Liu, Y.; Ruiz, M.T.; Lataire, E.; Vantorre, M.; Chen, C.; Zou, Z. Hybrid method for predicting ship manoeuvrability in regular waves. *Am. Soc. Mech. Eng. (ASME)* **2019**, *143*, 021203.
6. Kim, D.; Tezdogan, T.; Incecik, A. Hydrodynamic analysis of ship manoeuvrability in shallow water using high-fidelity URANS computations. *Appl. Ocean Res.* **2022**, *123*, 103176. [CrossRef]
7. Kim, D.; Song, S.; Jeong, B.; Tezdogan, T. Numerical evaluation of a ship's manoeuvrability and course keeping control under various wave conditions using CFD. *Ocean Eng.* **2021**, *237*, 109615. [CrossRef]
8. Cura-Hochbaum, A. On the numerical prediction of the ship's manoeuvring behaviour. *Ship Sci. Technol.* **2011**, *5*, 27–39. [CrossRef]
9. Hajivand, A.; Mousavizadegan, H.S. Virtual simulation of maneuvering captive tests for a surface vessel. *Int. J. Nav. Archit. Ocean Eng.* **2015**, *7*, 848–872. [CrossRef]
10. Sukas, O.F.; Kinaci, O.K.; Bal, S. System-based prediction of maneuvering performance of twin-propeller and twin-rudder ship using a modular mathematical model. *Appl. Ocean Res.* **2019**, *84*, 145–162. [CrossRef]
11. Simonsen, C.D.; Stern, F. Verification and validation of RANS maneuvering simulation of Esso Osaka: Effects ofdrift and rudder angle on forces and moments. *Comput. Fluids* **2003**, *32*, 1325–1356. [CrossRef]
12. Toxopeus, S.L. Verification and validation of calculations of the viscous flow around KVLCC2M in oblique motion. In Proceedings of the 5th Osaka Colloquium on Advanced CFD Applications to Ship Flow and Hull Form Design, Osaka, Japan, 14–15 March 2005.
13. Ismail, F.; Carrica, P.M.; Xing, T. Evaluation oflinear and nonlinear convection schemes on multidimensional non-orthogonal grids with applications to KVLCC2 tanker. *Int. J. Numer. Methods Fluids* **2010**, *64*, 850–886.
14. Islam, M.; Jahra, F.; Ryan, R.; Molyneux, D.; Hedd, L. Hydrodynamic performance of a FPSO in highly oblique flow conditions. In Proceedings of the ASME 34th International Conference on Ocean, Offshore and Arctic Engineering, St. John's, NL, Canada, 31 May–5 June 2015.
15. Davidson, K.S.M. The steering of ships in following seas. In Proceedings of the Sixth International Conference for Applied Mechanics, Rotterdam, The Netherland, 21–30 June 1948; Volume 2, pp. 554–568.
16. Ayaz, Z.; Vassalos, D.; Spyrou, K.J. Manoeuvring behaviour of ships in extreme astern seas. *Ocean Eng.* **2006**, *33*, 2381–2434. [CrossRef]
17. Chillcce, G.; el Moctar, O. A numerical method for manoeuvring simulation in regular waves. *Ocean Eng.* **2018**, *170*, 434–444. [CrossRef]
18. Lee, J.-H.; Kim, Y. Study on steady flow approximation in turning simulation of ship in waves. *Ocean Eng.* **2020**, *195*, 106645. [CrossRef]
19. Zhang, W.; Zou, A.-J.; Deng, D.-H. A study on prediction of ship maneuvering in regular waves. *Ocean Eng.* **2017**, *137*, 367–381. [CrossRef]

20. Wang, J.; Wan, D.; Yu, X. Standardzigzag maneuver simulations in calm water and waves withdirect propeller and rudder. In Proceedings of the 27th International Ocean and Polar Engineering Conference, San Francisco, CA, USA, 25–30 June 2017.
21. Umeda, N.; Hashimoto, H. Qualitative aspects of nonlinear ship motions in following and quartering seas with high forward velocity. *J. Mar. Sci. Technol.* **2002**, *6*, 111–121. [CrossRef]